11

Applications of Tilted-Pulse-Front Excitation

József András Fülöp and János Hebling
University of Pécs, Department of Experimental Physics
Hungary

1. Introduction

Tilting the pump pulse front has been proposed for efficient phase-matched THz generation by optical rectification of femtosecond laser pulses in $LiNbO_3$ (Hebling et al., 2002). By using amplified Ti:sapphire laser systems for pumping, this technique has recently resulted in generation of near-single-cycle THz pulses with energies on the 10-μJ scale (Yeh et al., 2007, Stepanov et al., 2008). Such high-energy THz pulses have opened up the field of sub-picosecond THz nonlinear optics and spectroscopy (Gaal et al., 2006, Hebling et al., 2008a).

The method of tilted-pulse-front pumping (TPFP) was introduced as a synchronization technique between the optical pump pulse and the generated THz radiation. Synchronization was accomplished by matching the group velocity of the optical pump pulse to the phase velocity of the THz wave in a noncollinear propagation geometry. Originally, TPFP was introduced for synchronization of amplified and excitation pulses in so called traveling-wave laser amplifiers (Bor et al., 1983). By using such traveling-wave excitation (TWE) of laser materials, especially dye solutions, extremely high gain (10^9) and reduced amplified spontaneous emission could be obtained (Hebling et al., 1991).

Contrary to the case of TWE, when TPFP is used for THz generation by optical rectification, a wave-vector (momentum) conservation condition or, equivalently, a phase-matching condition has to be fulfilled. It was shown (Hebling et al., 2002), that such condition is automatically fulfilled if the synchronization (velocity matching) is accomplished. The reason is that in any tilted pulse front there is present an angular dispersion of the spectral components of the ultrashort light pulse and there is a unique connection between the tilt angle of the pulse front and the angular dispersion (Bor & Rácz, 1985, Martínez 1986, Hebling 1996).

Angular dispersion was introduced into the excitation beam of so called achromatic frequency doubler (Szabó & Bor, 1990, Martínez, 1989) and sum-frequency mixing (Hofmann et al., 1992) setups in order to achieve broadband frequency conversion and keeping the ultrashort pulse duration. It was pointed out that in non-collinear phase-matched optical parametric generators (OPG) and optical parametric amplifiers (OPA) tilted pulse fronts are expected (Di Trapani et al., 1995). TPFP was used in the non-collinear OPA (NOPA) producing sub-5-fs pulses (Kobayashi & Shirakawa, 2000). The different aspect of tilted pulse front and angular dispersion is usually not mentioned in these papers dealing with broadband frequency conversion.

It is well known that the bandwidth of parametric processes is connected to the relative group velocities of the interacting pulses (Harris, 1969). Phase matching to first order in frequency

Source: Recent Optical and Photonic Technologies, Book edited by: Ki Young Kim,
ISBN 978-953-7619-71-8, pp. 450, January 2010, INTECH, Croatia, downloaded from SCIYO.COM

can also be formulated as matching the group velocities of (some of) the interacting pulses. In schemes utilizing angular dispersion for broadband frequency conversion it is important to consider the effect of angular dispersion on the group velocity for a precious connection between the Fourier-domain and the spatio-temporal descriptions.
In this Chapter, we give a comprehensive overview of the different types of applications relying on TPFP or angular dispersion with an emphasis on THz generation. The connection between pulse front tilt, group velocity and angular dispersion will be discussed for each type of application. The Chapter is organized as follows.
The introduction is followed by a discussion of the connection between pulse front tilt, group velocity and angular dispersion. The main part of the Chapter deals with the different types of applications. For the sake of simplicity we start with the applications relying on synchronization by tilting the pulse front. These include traveling-wave excitation of dye lasers, as well as possible future applications such as traveling-wave excitation of short-wavelength x-ray lasers, and ultrafast electron diffraction. Subsequently, applications based on achromatic phase matching for broadband frequency conversion will be discussed. Finally, high-field THz pulse generation by optical rectification of femtosecond laser pulses with tilted pulse front and its application to a new field of research, nonlinear THz optics and spectroscopy will be reviewed.

2. Pulse front tilt, group velocity, and angular dispersion

Tilting of the pulse front of picosecond pulses after traveling through a prism (Topp & Orner, 1975) or diffracting off a grating (Schiller & Alfano, 1980) was early recognized. Later, the following expression was deduced between the angular dispersion $\mathrm{d}\varepsilon/\mathrm{d}\lambda$ and the pulse front tilt γ created by the prism or the grating (Bor & Rácz, 1985):

$$\tan\gamma = -\bar{\lambda}\frac{\mathrm{d}\varepsilon}{\mathrm{d}\lambda}, \tag{1}$$

where γ is the tilt angle (the angle between the pulse front and the phase front, see Fig. 1), $\bar{\lambda}$ is the mean wavelength and $\mathrm{d}\varepsilon/\mathrm{d}\lambda$ is the angular dispersion. It was also shown that for a grating immersed in a material Eq. (1) has to be modified as (Szatmári et al., 1990):

$$\tan\gamma = -\frac{n}{n_g}\bar{\lambda}\frac{\mathrm{d}\varepsilon}{\mathrm{d}\lambda}, \tag{2}$$

where n and n_g are the (phase) index of refraction and the group index of the material, respectively.
A device-independent derivation of Eqs. (1) and (2) is possible (Hebling, 1996) for ultrashort light pulses having large beam sizes. In this case the short pulse consists of plane-wave monochromatic components with different frequencies (wavelengths). Such a case is illustrated schematically in Fig. 2 assuming that the beam propagates, and has an angular dispersion in the *x*-*z* plane. Hence, the phases of the spectral components are independent of the third (*y*) coordinate, and the electric field of the components can be described as:

$$E_\omega(x,z,t) = E_\omega \cdot \sin(\omega t - k_x x - k_z z + \varphi_0) \tag{3}$$

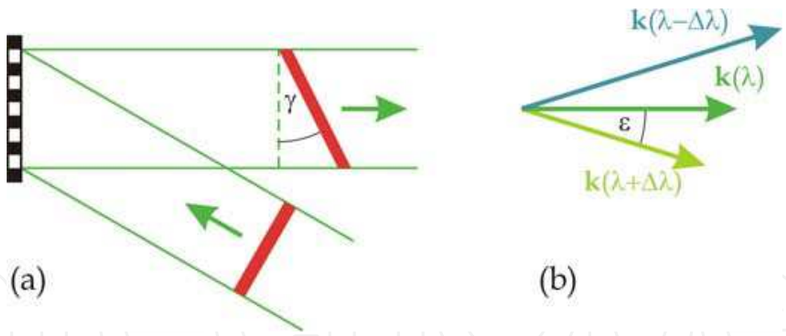

Fig. 1. (a) Pulse front tilt created by an optical element with angular dispersion (grating). (b) The corresponding angular dispersion of the wave vectors of the different spectral components of the ultrashort pulse.

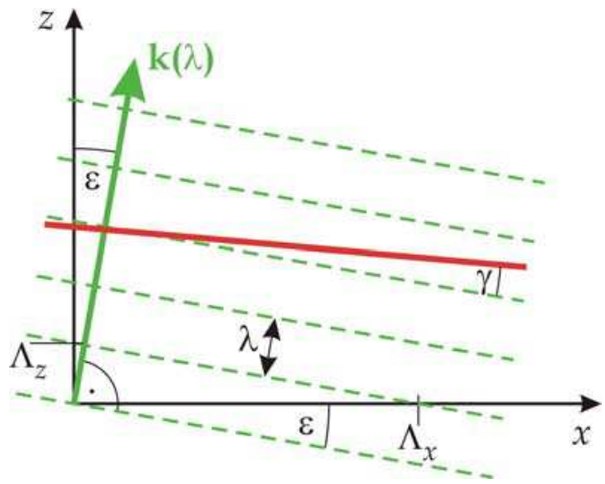

Fig. 2. Phase fronts (dashed lines) and pulse front (continuous line) for a light beam dispersed in the z–x plane. The phase front is indicated only for the mean wavelength. For different wavelengths the phase fronts are tilted relative to this. Positive angles are measured clockwise: $\varepsilon > 0$ and $\gamma < 0$.

Here $k_x = 2\pi/\Lambda_x = (2\pi/\lambda)\cdot\sin\varepsilon$ and $k_z = 2\pi/\Lambda_z = (2\pi/\lambda)\cdot\cos\varepsilon$ are the two components of the wave-vector, ε is the angle of propagation measured from the z-axis as shown in Fig. 2, and $\omega = 2\pi/\lambda$ is the angular frequency. Since for a phase front (a surface with constant phase) the argument of the sine function in Eq. (3) is constant, the slope of the phase front is given by:

$$m = -\frac{k_x}{k_z} = -\tan\varepsilon\ . \tag{4}$$

The pulse front at any time is the surface consisting of the points where the light intensity has a maximum. The intensity has maximum at points where the plane wave components with different frequencies have the same phase, i.e. where the derivative of the phase (the argument of the sine function in Eq. (3)) with respect to frequency is equal to zero. The result of such derivation is that the pulse front is plane with a slope of:

$$m_g = -\tan\gamma = -\tan\varepsilon + \frac{k_z}{\cos^2\varepsilon}\cdot\frac{\mathrm{d}\varepsilon}{\mathrm{d}k_z}\,, \tag{5}$$

where Eq. (4) was also used. If we choose the coordinate-system such that the main component propagates parallel to the z-axis, ε becomes equal to zero. With this choice, and by introducing the angular dispersion $\mathrm{d}\varepsilon/\mathrm{d}\lambda$ instead of $\mathrm{d}\varepsilon/\mathrm{d}k_z$, Eq. (5) reduces to Eq. (1). Since it was not necessary to suppose anything about the device which created the angular dispersion, with the above derivation we proved that the relation between the angular dispersion and the pulse front tilt as given in Eq. (1) is universal.

In order to prove the more general relationship given by Eq. (2) we suppose that the beam with angular dispersion propagates in a medium with wavelength (frequency) dependent index of refraction $n(\lambda)$. In this case the two components of the wave-vector of the plane wave, propagating in the direction determined by ε, are given by $k_x = 2\pi n(\lambda)/\Lambda_x =$ $= \left[2\pi n(\lambda)/\lambda\right]\cdot\sin\varepsilon$ and $k_z = 2\pi n(\lambda)/\Lambda_z = \left[2\pi n(\lambda)/\lambda\right]\cdot\cos\varepsilon$, respectively. By using these wave-vector components in the same derivation as above, one obtains Eq. (2) (Hebling, 1996). Again, since the derivation is independent of any device parameters, the relationship between the angular dispersion and the pulse front tilt as given by Eq. (2) is universal.

We can easily obtain (the reciprocal of) the group velocity of a short light pulse in the presence of angular dispersion. To this end we rewrite k_z by introducing the frequency instead of the wavelength as independent variable:

$$k_z = \frac{n(\omega)\omega}{c}\cos\varepsilon\,. \tag{6}$$

Since the group velocity is equal to the derivative of the angular frequency with respect to the wave vector (Main, 1978), we obtain for the reciprocal of the (sweep) group velocity along the z axis:

$$v_{\mathrm{g}}^{-1} = \frac{\mathrm{d}k_z}{\mathrm{d}\omega} = \frac{1}{c}\left[n\cdot\cos\varepsilon + \omega\left(\cos\varepsilon\cdot\frac{\mathrm{d}n}{\mathrm{d}\omega} - \sin\varepsilon\cdot n\cdot\frac{\mathrm{d}\varepsilon}{\mathrm{d}\omega}\right)\right]. \tag{7}$$

Although this depends on the angular dispersion, the reciprocal of the group velocity is independent of it. Really, using $\varepsilon = 0$ in Eq. (7) results in the well known expression:

$$v_{\mathrm{g}}^{-1} = \frac{1}{c}\left(n + \omega\cdot\frac{\mathrm{d}n}{\mathrm{d}\omega}\right) = \frac{n_{\mathrm{g}}}{c}\,, \tag{8}$$

where $n_{\mathrm{g}} = c/v_{\mathrm{g}}$ is the usual group index.

It is important to notice that the frequency derivative of the reciprocal of the group velocity depends on the angular dispersion. The most important and well known implication of this is the working of pulse compressors consisting of prism or grating pairs. In such compressors angular dispersion is present in the light beam during the path between the two dispersive elements (prisms or gratings). The (negative) group delay dispersion (GDD) of such compressor is given as:

$$\mathrm{GDD} = l\cdot\frac{\mathrm{d}v_{\mathrm{g}}^{-1}}{\mathrm{d}\omega}\,, \tag{9}$$

where l is the distance between the dispersive elements along the beam path. According to this, by taking the frequency derivative of the reciprocal of the group velocity as given by Eq. (7), substituting $\varepsilon = 0$ and multiplying by l result in the general expression for the GDD caused by propagation in the presence of angular dispersion:

$$\mathrm{GDD} = \frac{l}{c} \cdot \left[2 \cdot \frac{\mathrm{d}n}{\mathrm{d}\omega} + \omega \cdot \frac{\mathrm{d}^2 n}{\mathrm{d}\omega^2} - \omega \cdot n \cdot \left(\frac{\mathrm{d}\varepsilon}{\mathrm{d}\omega} \right)^2 \right], \tag{10}$$

in accordance with (Martínez et al., 1984). For the case of prism or grating compressors, with a large accuracy, $n \equiv 1$ and Eq. (10) simplifies to Eq. (10b), and the GDD is always negative:

$$\mathrm{GDD} = -\frac{l \cdot \omega}{c} \cdot \left(\frac{\mathrm{d}\varepsilon}{\mathrm{d}\omega} \right)^2 . \tag{10b}$$

When pulse front tilt (or equivalently, angular dispersion) is introduced into a beam of ultrashort pulses in order to achieve achromatic frequency conversion or synchronization of pump and generated pulses (see examples below), $n \not\equiv 1$ in the medium, and the full expression of Eq. (10) has to be considered. Since the first and second terms on the right hand side of Eq. (10) are usually positive, and the third term always negative, the effect of the angular dispersion and the material dispersion can sometimes compensate each other. If, however, a very large angular dispersion is needed the third term becomes much higher than the first two ones, and it causes a rapid change of the pulse length during propagation hindering efficient frequency conversion.

In the above derivation plane wave components with infinite transversal extension were assumed. For finite beam sizes a more complicated derivation (Martínez, 1986) is needed. According to this, the tilt angle changes with propagation distance and besides angular dispersion also spatial dispersion will be present. The spatio-temporal distortions in this case are described and investigated by an elegant theory (Akturk et al., 2005). According to numerical calculations, however, such distortions are usually not significant on a distance smaller than the beam size. This condition is typically fulfilled in frequency conversion processes of high-energy ultrashort pulses.

Finally, we have to recognize that a strong restriction was used in the above discussions, namely, an isotropic index of refraction was assumed. However, it is well known that in frequency conversion processes at least one of the beams involved has extraordinary polarization with a refractive index depending on propagation direction. (The only possible exception is quasi-phase-matching.) Because of this, it is essential to re-consider the above derivations. Let us first investigate again the group index! If we just apply the definition of the group index as it was introduced in Eq. (8) and take into account that besides the explicit frequency dependence of the refractive index, in the presence of angular dispersion an implicit dependence $n^*(\omega) = n\left(\omega, \varepsilon(\omega)\right)$ can also be present, we obtain:

$$v_{\mathrm{g}}^{-1} = \frac{1}{c}\left(n^* + \omega \cdot \frac{\mathrm{d}n^*}{\mathrm{d}\omega} \right) = \frac{1}{c}\left(n + \omega \cdot \frac{\partial n}{\partial \omega} + \omega \cdot \frac{\partial n}{\partial \varepsilon} \cdot \frac{\mathrm{d}\varepsilon}{\mathrm{d}\omega} \right) = \frac{1}{c}\left(n_{\mathrm{g}} + \omega \cdot \frac{\partial n}{\partial \varepsilon} \cdot \frac{\mathrm{d}\varepsilon}{\mathrm{d}\omega} \right) = \frac{n_{\mathrm{g}}^*}{c} . \tag{11}$$

According to Eq. (11), in the presence of angular dispersion (which is in a plane containing the optical axis) an n_{g}^* modified group index is effective. Depending on the signs of the

angular dependence of the refractive index and that of the angular dispersion, the effective group index can be either larger or smaller than the (usual, material) group index. Furthermore, the value of the effective group index and that of the group velocity can be set by adjusting the angular dispersion. (A more rigorous derivation staring from Eq. (7) results in the same expression as Eq. (11).) We note that even though extraordinary propagation of an angularly dispersed beam is a common situation in many types of frequency conversion schemes (see Section 4), not much attention has been payed previously to generalize the definition of group velocity to such a case.
Describing the angular dispersion with the frequency dependence of the angle instead of its wavelength dependence, the relation between the pulse front tilt angle and the angular dispersion becomes:

$$\tan\gamma = \frac{n}{n_{\mathrm{g}}}\bar{\omega}\frac{\mathrm{d}\varepsilon}{\mathrm{d}\omega}. \tag{2b}$$

By using a similar calculation as above, it is easy to show that for anisotropic materials Eq. (2b) is modified similarly to the modification of the group velocity:

$$\tan\gamma = \frac{n}{n_{\mathrm{g}}^{*}}\bar{\omega}\frac{\mathrm{d}\varepsilon}{\mathrm{d}\omega}. \tag{12}$$

Both the group velocity and the tangent of the tilt angle are changing by a factor of $n_{\mathrm{g}} / n_{\mathrm{g}}^{*}$ in presence of angular dispersion in anisotropic materials.
In conclusion, if in the beam of an ultrashort pulse angular dispersion is present, then necessarily a pulse front tilt is also present. Eq. (12) gives the relationship between the pulse front tilt and the angular dispersion. Furthermore, we have shown that contrary to the isotropic case, for anisotropic media the group velocity of the light pulse depends on the angular dispersion, too. Hence, the group velocity can be adjusted by adjusting the angular dispersion. This is utilized in many broadband frequency conversion schemes where the group velocities of interacting pulses are matched in such a way. We will show examples for this in Section 4.

3. Pulse front tilt for synchronization

In the first group of applications of TPFP the tilt of the intensity front is used to achieve the same sweep velocity of the pump pulse along a surface or along a volume close to a surface as the velocity of the generated excitation (i.e. amplified spontaneous emission, or surface polariton), or to the velocity of an other pulse (i.e. electron packet). In this group of applications angular dispersion is not an issue.

3.1 Traveling-wave excitation of lasers

Tilted-pulse-front excitation for generation of amplified spontaneous emission (ASE) pulses in dye solutions was introduced in 1983 by two groups independently (Polland et al., 1983, Bor et al., 1983). Both groups applied transversal pumping geometry, that is the pump pulses illuminated the long side of the dye cell perpendicularly, and the generated ASE pulse propagated along the surface in the pencil-like excited volume (see Fig. 3). The

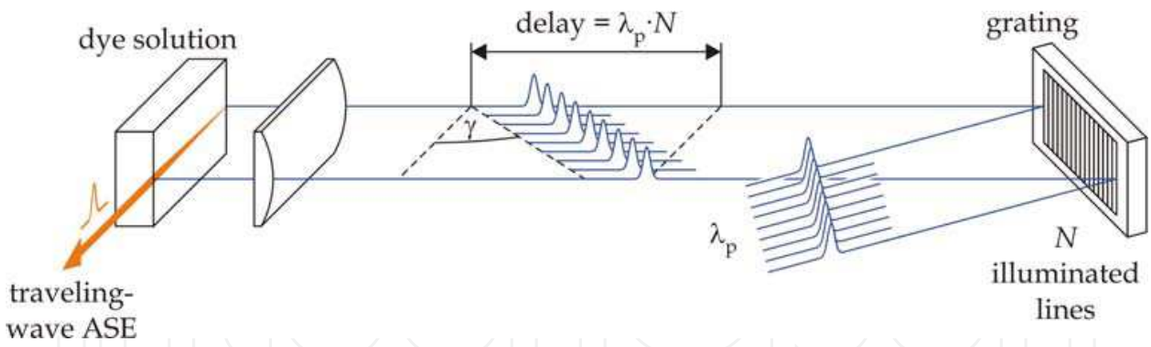

Fig. 3. Ultrashort (ps) light pulse generation by traveling-wave pumped ASE (Bor et al., 1983).

technique of diffracting the pump pulses off an optical grating was applied to create the tilted pulse front (Schiller & Alfano, 1980). The tilt angle γ was chosen to fulfill the condition $\tan\gamma = n_g$, where $n_g = c/v_g$ is the group refractive index of the dye solution at the mean ASE wavelength. In this way the pump pulse swept the surface of the dye solution with the group velocity of the ASE pulse inside the dye solution. This situation is called traveling-wave excitation(TWE). The exact temporal overlap between the pump pulse and the generated ASE pulse allowed an effective use of the pump energy even for dyes having excited state lifetimes of only a few ps. For example, 2% of the pump energy was converted into the energy of the ASE pulse for IR dyes that have less than 10^{-3} fluorescence quantum efficiency (Polland et al., 1983) due to the short lifetime dictated by fast non-radiative processes. The reason for the much higher energy conversion efficiency of the traveling-wave pumped amplifier as compared to the fluorescence quantum efficiency is that in the traveling-wave pumped amplifier the dye molecules are in excited state only for a short duration at every point of the amplifier because of the synchronism between the pump and the generated pulse. Another consequence of this is that the TWE resulted in two times shorter (6 ps) ASE pulse duration than that of the pump pulse (Bor et al., 1983). Using the TWE scheme in distributed feedback dye lasers resulted in sub-ps Fourier-transform limited pulses (Szabó et al. 1984).

It was also possible to use TWE efficiently with fs pump pulses (Hebling & Kuhl, 1989a, Hebling & Kuhl, 1989b, Klebniczki et al. 1990, Hebling et al., 1991). In these experiments TWE was achieved by non-perpendicular excitation and by the pulse front tilt introduced by a glass prism contacted to the dye cell, as shown in Fig. 4. By seeding the traveling-wave amplifier by white-light continuum pulses stretched in BK7 glass it was possible to generate about 100 fs long tunable pulses in the 640–680 nm range (Klebniczki et al., 1990). Furthermore, by seeding with attenuated continuous light of a Kr^+ laser, it was demonstrated, that the traveling-wave pumped dye amplifier can work as a gated amplifier with 100 fs gate window and as large as 10^9 gain (Hebling et al., 1991). According to the measurements as well as to model calculations for exact synchronisms the duration of the gate window is approximately equal to the pump pulse duration (somewhat shorter), while for different pump sweep and ASE pulse velocities it is equal to the difference of the times the pump and ASE pulses need to travel the length of the amplifier.

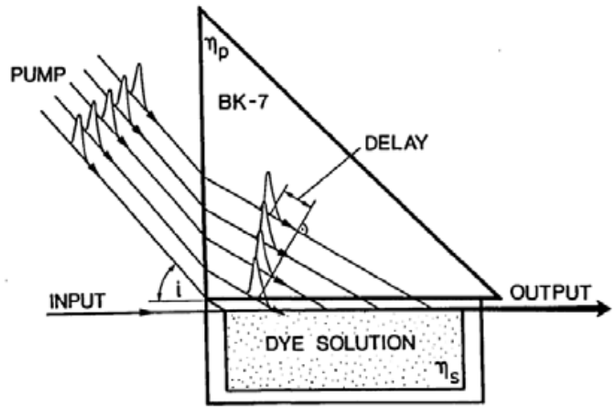

Fig. 4. Non-perpendicular TWE for ultrashort (fs) light pulse generation (Hebling et al., 1991).

3.2 Traveling-wave excitation of X-ray lasers

Laser action at extreme ultraviolet (XUV) and x-ray wavelengths is of great practical importance for many applications. For biological applications especially the so-called water window (4.4–2.2 nm) is of great interest. X-ray laser action can be achieved in highly ionized plasmas or in free electron lasers. Many plasma-based x-ray laser schemes use short laser pulses for creating the plasma and the population inversion required for x-ray lasing. In many cases reported so far, the pumping mechanism is either electron collisional excitation of neon-like or nickel-like ions, or inner-shell excitation or ionization processes (Daido, 2002, and references therein).

One of the main difficulties associated with x-ray lasing is the short lifetime of the excited states, which typically scales as λ^2 (Simon et al., 2005), where λ is the wavelength. In the 1 nm – 100 nm region, spontaneous transition rates correspond to 0.1 ps^{-1} – 10 ps^{-1} (Kapteyn, 1992). Processes with even shorter time constants, such as Auger decay of inner-shell vacancies with typical decay rates of 1 fs^{-1} – 10 fs^{-1}, can in many schemes impose further constraints on the required pumping rate (Kapteyn, 1992). Due to the short time available for the population inversion to build up, ultrashort pump pulses can be used to excite population inversion efficiently.

Due to the decreasing rate of stimulated emission with decreasing wavelength (Simon et al., 2005), in order to obtain a useful output level from an x-ray laser it is essential to provide population inversion over sufficient length, typically a few millimeters up to a few centimeters. This, together with the short amount of time available for population inversion requires using ultrashort pump pulses with a traveling-wave pumping geometry, which provides exact synchronization between the pump pulse and the generated x-ray pulse.

Sher et al. (Sher et al., 1987) have used grazing incidence excitation for nearly synchronous traveling-wave pumping of an XUV laser at 109 nm wavelength in Xe (Fig. 5). Later, a modified setup with grating-assisted traveling-wave geometry was used, where a grating pair introduced a small tilt of the pump pulse front for more exact pump-XUV synchronization (Barty, et al., 1988). However, in these early experiments a grooved target had to be used in order to compensate for the reduced pumping efficiency caused by the grazing incidence geometry. Kawachi et al. (Kawachi, et al., 2002) employed a quasi traveling-wave pumping scheme using a step mirror, which was installed in the line-

focusing system to excite the nickel-like silver and tin x-ray lasers at the wavelengths of 13.9 and 12.0 nm.

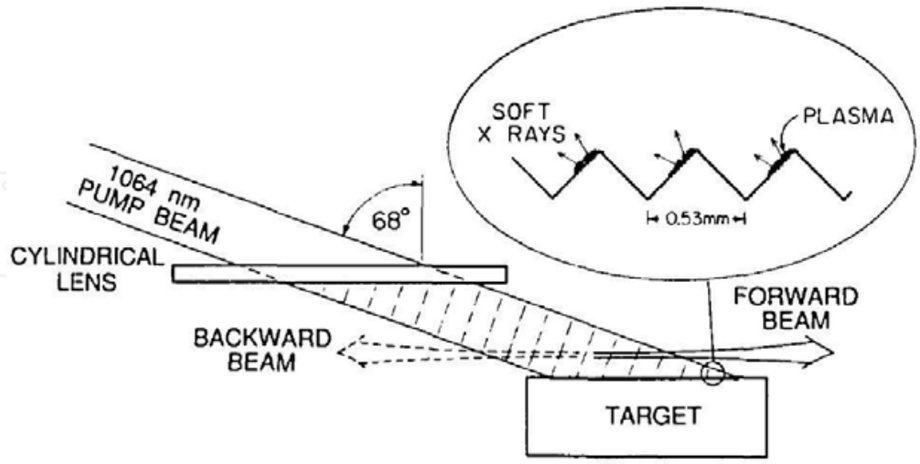

Fig. 5. Grazing incidence x-ray laser pumping scheme (Sher, et al., 1987).

On the way towards achieving x-ray lasing from laser produced plasmas with photon energies approaching the keV milestone, an important step, besides the investigation of fundamental physics concerned with the creation of population inversion, is to develop extremely accurate and controllable traveling-wave pumping systems (Daido, 2002). We would like to emphasize that the existing technique of tilted-pulse-front pumping (see Section 5) can provide the required tools for pump–x-ray synchronization with femtosecond accuracy. It also allows for working with perpendicular incidence of the pump beam onto the target. This gives higher effective pump intensity due to reduced pump spot size and due to improved energy coupling-in efficiency allowed by the reduced reflection coefficient from the plasma surface. A possible experimental setup is shown in Fig. 6. The pulse-front-tilting setup made up of a grating and a spherical focusing lens is extended by a concave cylindrical lens, which shifts the focus of the pump beam introduced by the spherical lens to the surface of the target by its defocusing effect in the direction perpendicular to the plane of the drawing. Thus, in the plane of the drawing a line focus is generated at the target. The pump intensity can also be increased by using demagnifying imaging.

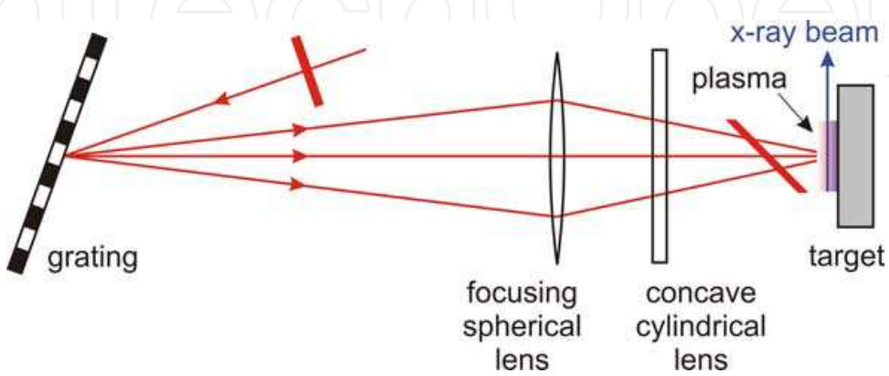

Fig. 6. Tilted-pulse-front pumping scheme for exactly synchronized excitation of an x-ray laser from laser-produced plasma.

3.3 Ultrafast electron diffraction

In recent years it became possible to achieve atomic-scale resolution simultaneously in time and space in revealing structures and dynamics. One important tool for such high-resolution studies is ultrafast electron diffraction and microscopy (Baum & Zewail, 2006). In these techniques an ultrashort (femtosecond) laser pulse is used to initiate a change in the sample. The dynamics is probed by an ultrafast electron pulse. Besides the temporal spread of the electron pulse due to space charge effect the difference in the group velocities of the optical and the electron pulses can impose an often more severe limitation on the temporal resolution (Fig. 7(a)). This mismatch in the propagation velocities along the sample becomes especially significant in case of ultrafast electron crystallography, where the electrons probe the sample at grazing incidence and the laser pulse triggering the dynamics has (nearly) perpendicular incidence (Fig. 7(b)).

Baum & Zewail (Baum & Zewail, 2006) proposed to use a traveling-wave type excitation scheme with tilted laser pulse front for exact synchronization with the probing electron pulse (Fig. 7(c–e)). They demonstrated a 25-fold reduction in time spread. They also discuss limitations in time resolution due to the possible curvature of the tilted pulse front. Furthermore, they proposed tilting the electron packet (generated by a tilted optical pulse illuminating a photocathode) to overcome space charge problems that are especially important in single-shot experiments.

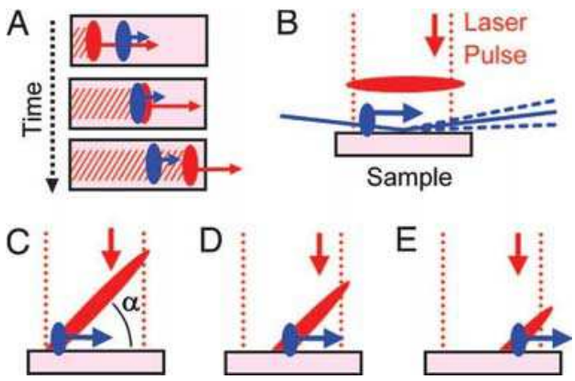

Fig. 7. (a) Group velocity mismatch in ultrafast electron diffraction. (b) Ultrafast electron crystallography without laser pulse front tilt. (c–e) Traveling-wave excitation of the sample by tilting the optical pump pulse front for synchronization with the slow (33% of *c*) electron pulse (Baum & Zewail, 2006). Copyright 2006 National Academy of Sciences, U.S.A.

4. Achromatic phase matching

In this part we consider various achromatic phase matching schemes used for frequency conversion or parametric amplification of ultrashort laser pulses. In this group of applications angular dispersion plays a key role, which affects the bandwidth of nonlinear processes. It was early recognized that achromatic phase matching is related to group velocity matching of the interacting pulses (Harris, 1969). An often neglected aspect in such schemes is the pulse front tilt linked to angular dispersion. The following discussion will include this aspect, too.

In frequency conversion of ultrashort laser pulses the bandwidth of the nonlinear material is of crucial importance. In nonlinear processes such as second- and third-harmonic generation,

sum-frequency generation, optical parametric amplification, etc., broadband phase matching usually requires the use of thin nonlinear crystals. This, in turn, seriously limits the efficiency of frequency conversion. One way to overcome this limitation is to adopt the technique of achromatic phase matching to frequency conversion of ultrashort laser pulses.

Many different schemes have been proposed and used for various nonlinear optical processes with ultrashort laser pulses. The theoretical analysis of these schemes was carried out in most cases either in the Fourier domain (in terms of wave vectors and frequencies) or in the spatio-temporal domain. Little or no attention was paid to the connection of the two distinct descriptions. Even though descriptions in the two domains are equivalent, to consider the connection between them gives a more complete picture and can, in some cases, reveal new important features, which can be relevant for designing an experimental setup. As examples, in the following we will consider collinear and non-collinear achromatic second-harmonic generation (SHG), non-collinear achromatic sum-frequency generation (SFG), and NOPA with and without angular dispersion of the signal beam.

4.1 Collinear achromatic SHG

Achromatic phase matching in nonlinear frequency conversion was originally introduced for automatic, i.e. alignment-free phase matching in second harmonic generation (SHG) of tunable monochromatic laser sources (Saikan, 1976; see also references in Szabó & Bor, 1990). The technique relies on sending the pump beam at each wavelength through a birefringent nonlinear crystal under its respective phase-matching angle, which varies with wavelength. To this end, an element with appropriate angular dispersion was used in front of the crystal. In such a way the effective bandwidth of the nonlinear crystal could be increased considerably.

The femtosecond frequency doubler proposed independently by Szabó & Bor (Szabó & Bor, 1990; Szabó & Bor, 1994) and Martínez (Martínez, 1989) adopts the principle of automatic phase matching to ultrashort pulses. It utilizes the angular dispersion of gratings to achieve collinear achromatic phase matching in the nonlinear crystal and, subsequently, to eliminate the angular dispersion from the generated second-harmonic radiation (Fig. 8).

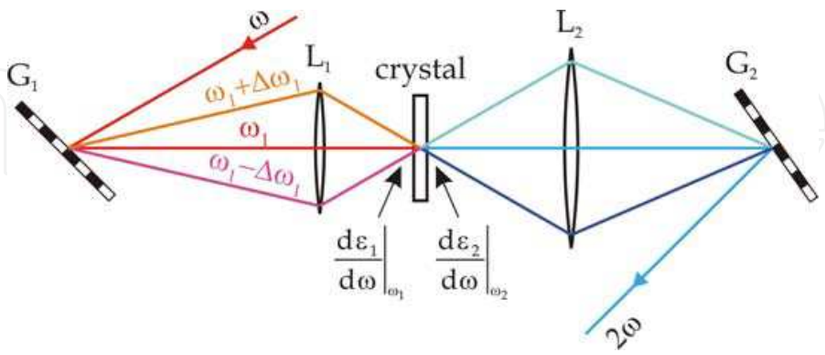

Fig. 8. Femtosecond frequency doubler based on collinear achromatic phase matching (Szabó & Bor, 1990). G_1, G_2: gratings, L_1, L_2: lenses.

Martínez (Martínez, 1989) gave a thorough analysis of the scheme in the Fourier-domain, without discussing the spatio-temporal implications. The achromaticity of the scheme relies on sending each fundamental frequency component into the crystal under its respective

phase-matching angle. The phase matching condition at the fundamental and second harmonic central frequency components ω_1 and $\omega_2 = 2\omega_1$, respectively, reads as:

$$\mathbf{k}_2(\omega_2 = 2\omega_1) = 2\mathbf{k}_1(\omega_1), \tag{13}$$

where $\mathbf{k}_1$ and $\mathbf{k}_2$ are the fundamental and second harmonic wave vectors, respectively. Their magnitude is given by $k_i(\omega) = \omega_i \cdot n_i(\omega)/c$ with $i = 1, 2$. Eq. (13) implies that $n_1(\omega_1) = n_2(\omega_2)$. The condition for achromatic phase matching can be given as follows:

$$\mathbf{k}_2(\omega_2' = 2\omega_1 + \Delta\omega_1 + \Delta\omega_1') = \mathbf{k}_1(\omega_1 + \Delta\omega_1) + \mathbf{k}_1(\omega_1 + \Delta\omega_1'), \tag{14}$$

where $\Delta\omega_1$ and $\Delta\omega_1'$ are arbitrary detunings from the fundamental central frequency. Martínez showed that Eq. (14) implies

$$\left.\frac{\mathrm{d}n_1^*}{\mathrm{d}\omega}\right|_{\omega_1} = 2 \cdot \left.\frac{\mathrm{d}n_2^*}{\mathrm{d}\omega}\right|_{\omega_2}. \tag{15}$$

Please note that by writing n^* rather than simply n in Eq. (15), we allow that any of the two pulses may have extraordinary propagation. (In case of birefringent phase matching at least one of them must, in fact, be extraordinary.) In practical setups, such as that in Fig. 8, the required angular dispersion is usually matched only to first order by the dispersive optics and higher-order mismatch still imposes bandwidth limitation. Matching of angular dispersion to higher order was demonstrated with optimized setups and tunable cw lasers (Richman et al., 1998).

It is now straightforward to find the connection to the spatio-temporal description of the arrangement. According to Eq. (11), and the phase matching condition $n_1(\omega_1) = n_2(\omega_2)$ together with Eq. (15) imply that the fundamental and the second-harmonic group velocities are matched: $v_{g1} = v_{g2}$. On the other hand, it follows from the collinear geometry for each $(\omega_1', 2\omega_1')$ frequency pair (Fig. 8) that the angular dispersion of the fundamental is twice that of the second harmonic:

$$\left.\frac{\mathrm{d}\varepsilon_1}{\mathrm{d}\omega}\right|_{\omega_1} = 2 \cdot \left.\frac{\mathrm{d}\varepsilon_2}{\mathrm{d}\omega}\right|_{\omega_2}, \tag{16}$$

where $\varepsilon(\omega)$ is the angle between the optic axis and the wave vector of the respective frequency component. By using s, the matching of group velocities $v_{g1} = v_{g2}$, and Eqs. (12) and (16), one obtains that also the fundamental and second-harmonic pulse fronts are matched: $\gamma_1 = \gamma_2$.

In summary, we have shown that for the collinear SHG scheme (Fig. 8) achromatic phase matching to first order is equivalent to simultaneous group-velocity and pulse-front matching between the fundamental and the generated SHG pulses. Pulse-front matching allows the scheme to be used with large beam sizes.

4.2 NOPA

In recent years the technique of OPA (see e.g. Cerullo & De Silvestri, 2003, and references therein) has opened up a new path towards generating few-cycle laser pulses with

unprecedented peak powers. Such pulses are crucial for the investigation of laser-driven strong-field phenomena, having become an accessible field of research with the advent of suitable laser systems.

In the OPA process phase-matching in a non-collinear geometry (NOPA) allows for extremely large amplification bandwidths, and thereby enables the amplification of broadband seed pulses using relatively narrowband pump pulses delivered by conventional laser amplification technology. Usually, a narrowband pump pulse is used, and the signal is stretched in time. The non-collinearity angle between signal and pump introduces an additional adjustable parameter besides the crystal orientation angle, which allows achieving phase matching to first order in signal frequency (achromatic phase matching). In such a setup the broadband signal beam has no angular dispersion while the idler beam generated in the amplification process has one. In such a scheme, achromatic phase matching is related to matching the (projected) group velocities of the signal and the idler pulses. Due to the long pulse durations, pulse front matching is usually not a practical issue.

Recently, the use of short (few-ps to sub-ps) pump pulses was proposed for generation of high-power few-cycle pulses (Fülöp et al., 2007, Major et al., 2009). In such a high-energy short-pulse-pumped NOPA pulse front matching between signal and pump is crucial to enable amplification with large beam sizes. This can be conveniently accomplished by introducing a small amount of angular dispersion into the pump (Kobayashi & Shirakawa, 2000, Fülöp et al., 2007).

As the above examples show, achromatic phase matching can also be achieved without appropriate pulse front matching in certain schemes. Therefore, in case of large beam sizes, which is the typical situation in high-power applications, it is important to consider both the Fourier domain as well as the spatio-temporal domain when designing frequency converting or OPA stages.

4.3 Non-collinear achromatic SFG

In NOPA schemes an additional degree of freedom can be provided by introducing angular dispersion into the signal beam. As we will show below, in such a scheme simultaneous group velocity and pulse front matching is achieved for all three interacting pulses in case of achromatic phase matching. We will discuss the scheme as achromatic SFG (the inverse process of OPA), which makes its symmetry with respect to signal and idler more obvious. The results are valid both for NOPA and SFG.

A special case of achromatic SFG is the non-collinear SHG scheme with two identical input beams proposed by Zhang et al. (Zhang et al., 1990), which utilizes the angular dispersion of prisms for achromatic phase matching. Each of the two incoming beams of the same central frequency ω_1 is dispersed in separate prisms to have angular dispersions equal in magnitudes but opposite in signs. The dispersed beams enter the nonlinear crystal under opposite angles of incidence. The emerging second-harmonic beam propagates along the angle bisector of the input beams and has no angular dispersion. Zhang et al. showed that simultaneous phase and group velocity matching is possible in such a scheme in BBO.

In the non-collinear achromatic SFG scheme shown in Fig. 9 two ultrashort pulses with central frequencies ω_1 and ω_2 are entering the nonlinear crystal under different angles α_1 and α_2, respectively. These non-collinearity angles are measured from the propagation direction of the generated SFG beam having the central frequency $\omega_3 = \omega_1 + \omega_2$. The incidence angles and the angular dispersions $\mathrm{d}\alpha_1 / \mathrm{d}\omega\big|_{\omega_1}$ and $\mathrm{d}\alpha_2 / \mathrm{d}\omega\big|_{\omega_2}$ of the two

incoming beams are chosen such that the output SFG beam is generated with maximal bandwidth (achromatic phase matching) and without angular dispersion. The latter condition is important for practical applications of the scheme.

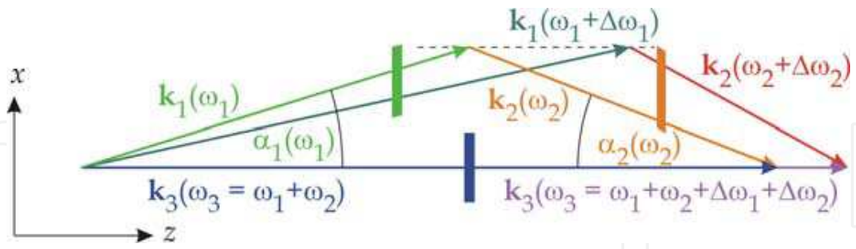

Fig. 9. Non-collinear achromatic SFG (or NOPA) scheme with angularly dispersed input beams. The corresponding pulse fronts are indicated by the vertical bars.

Let us first consider the scheme in the Fourier domain. The phase matching condition at the central frequencies can be described in terms of the wave vectors as

$$\mathbf{k}_3(\omega_3 = \omega_1 + \omega_2) = \mathbf{k}_1(\omega_1) + \mathbf{k}_2(\omega_2), \tag{17}$$

where $k_i(\omega) = |\mathbf{k}_i(\omega)| = \omega_i \cdot n_i(\omega)/c$ with $i = 1, 2, 3$, and n_i being the respective refractive index, which can be either ordinary or extraordinary. Depending on the type of phase matching one or more of the interacting beams propagate as extraordinary waves in the birefringent nonlinear medium. The condition for achromatic phase matching can be written as

$$\mathbf{k}_3(\omega_3' = \omega_1 + \omega_2 + \Delta\omega_1 + \Delta\omega_2) = \mathbf{k}_1(\omega_1 + \Delta\omega_1) + \mathbf{k}_2(\omega_2 + \Delta\omega_2), \tag{18}$$

where $\Delta\omega_1$ and $\Delta\omega_2$ are arbitrary detunings from the input central frequencies ω_1 and ω_2 within the bandwidth of the input pulses. The independent values of $\Delta\omega_1$ and $\Delta\omega_2$ reflect the fact that all possible combinations of the spectral components of the input pulses contribute to the SFG process. Since the generated SFG beam is not allowed to have any angular dispersion, the direction of $\mathbf{k}_3$ is along the *z*-axis for all sum-frequency components. Usually, in a practical setup it is sufficient to fulfill the achromatic phase matching condition, Eq. (18), only to first order in the frequency offsets $\Delta\omega_1$ and $\Delta\omega_2$. The non-collinearity angles α_1 and α_2, as well as the angular dispersions $\mathrm{d}\alpha_1/\mathrm{d}\omega|_{\omega_1}$ and $\mathrm{d}\alpha_2/\mathrm{d}\omega|_{\omega_2}$ can be found by decomposing Eq. (18) into components parallel with (*z*-axis) and perpendicular to (*x*-axis) $\mathbf{k}_3$, and by keeping only the zero- and first-order terms in the frequency offsets (first-order achromatic phase matching). Similar calculation was introduced by Martínez for collinear achromatic SHG (Martínez, 1989), as was discussed above in Section 4.1.

Let us now consider the spatio-temporal implications of Eq. (18), the achromatic phase matching condition. In the following we will outline the main results; details of the calculation will be given elsewhere (Fülöp & Hebling, to be published). The setup corresponding to the phase matching scheme shown in Fig. 9 is depicted in Fig. 10.

The terms first-order in $\Delta\omega_1$ and $\Delta\omega_2$ of the *x*-component of Eq. (18) imply the following relation between the incidence angles α_i and the corresponding angular dispersions $\mathrm{d}\alpha_i/\mathrm{d}\omega|_{\omega_i}$:

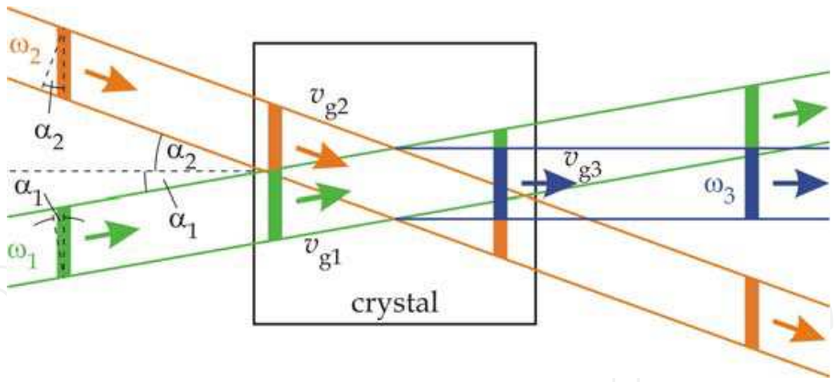

Fig. 10. Matching of the pulse fronts and the projected group velocities in the non-collinear achromatic SFG scheme. In case of NOPA the signal (ω_1) and pump (ω_3) beams are present at the input, and the idler (ω_2) is missing.

$$\tan(\alpha_i) = \frac{n_i}{n_{gi}^*}\omega_i \left.\frac{\mathrm{d}\alpha_i}{\mathrm{d}\omega}\right|_{\omega_i}, \quad (i = 1, 2). \tag{19}$$

Please note that it is the effective group index n_g^* which enters Eq. (19). By comparing Eq. (19) to Eq. (12) one can see that the incidence angles of the incoming beams are equal to their respective pulse front tilt angles γ: $\alpha_1 = \gamma_1$ and $\alpha_2 = \gamma_2$. Hence, the pulse fronts of both incoming beams are perpendicular to the propagation direction of the generated SFG beam (z-axis). This means that the pulse fronts of all three interacting pulses are matched to each other.

By expressing the angular dispersions from Eq. (19) and inserting them into the first-order z-component of Eq. (18), one obtains

$$v_{g1}\cos(\alpha_1) = v_{g2}\cos(\alpha_2) = v_{g3}. \tag{20}$$

Thus, the projections of the group velocities onto the z-axis are also matched. As shown in Fig. 10, both incoming pulses are propagating through the crystal with their own group velocities such that their pulse fronts are matched to each other as well as to that of the generated SFG pulse. In addition, the equal sweep velocity of all three pulses along the SFG propagation direction ensures that the generated SFG pulse has minimal pulse duration or, equivalently, maximal bandwidth. We also note that Eq. (20) together with the zero-order z-component of Eq. (18) lead to the following symmetric relation between the phase and group refractive indices:

$$\omega_1 n_1 n_{g1}^* + \omega_2 n_2 n_{g2}^* = \omega_3 n_3 n_{g3}^*. \tag{21}$$

In summary, we have shown that the achromatic phase matching condition for NOPA with angularly dispersed signal or for non-collinear SFG is equivalent to simultaneous pulse-front and group-velocity matching between all three interacting pulses. Hence, the scheme can be of interest for high-power (large beam cross section) applications, too.

We note that a calculation similar to that outlined above can be carried out for NOPA with a quasi-monochromatic pump (ω_3). The phase matching scheme of Fig. 9 can also be used

here with a single $\mathbf{k}_3$ vector representing the pump. Our calculations show that simultaneous group velocity and pulse front matching between signal (ω_1) and idler (ω_2) can be achieved in case of achromatic phase matching. It is not clarified yet if achromatic phase matching also allows for a possible pulse front mismatch.

5. Generation of THz pulses by optical rectification

In the last two decades a new branch of science, the terahertz (THz) science emerged (Tonouchi, 2007, Lee, 2009). Usually the 0.1-10 THz range of the electromagnetic spectrum is considered as THz radiation, earlier referred to as the far-IR range. The reason of the new name is justified by the fact that nowadays very frequently time-domain terahertz spectroscopy (TDTS) (Grischkowsky, 1990) based on single-cycle THz pulses is used for investigations. In this method the temporal dependence of the electric field in the THz pulse is measured rather than the intensity envelope. Usually in TDTS setups a biased photoconductive antenna creates the THz pulses and an unbiased one is used for detection. Both are triggered by ultrashort laser pulses. While these devices are well suited for linear absorption and index of refraction measurements the energy of the THz pulses generated by a usual photoconductive antenna is not enough for creating nonlinear effects. Because of this, pump-probe measurements and other applications need THz pulse sources of much higher energy.

Optical rectification (OR) of ultrashort laser pulses (Hu et al., 1990) is a simple and effective method for high-energy THz pulse generation. Similarly to other nonlinear optical frequency conversion methods, a phase-matching condition needs to be fulfilled also in OR. For OR this requires the same group velocity of the pump pulse than the phase velocity of the generated THz radiation. Most frequently ZnTe is used as electro-optic crystal for OR, since in this material velocity matching is accomplished for the 800-nm pulses of Ti:sapphire lasers (Löffler et al., 2005, Blanchard et al., 2007). In this way 1.5-μJ single-cycle THz pulses were produced (Blanchard et al., 2007). However, ZnTe has more than two times smaller figure of merit for THz generation than $LiNbO_3$ (LN). Furthermore, THz absorption of free carriers generated by two-photon absorption of the pump can seriously limit the applicable pump intensity and the generation efficiency in ZnTe (Hoffmann et al., 2007, Blanchard et al., 2007). So LN is a much more promising material for THz generation by OR. However, collinear phase-matching is not possible in LN since the group velocity of the (near-IR) pump is more than two times larger then the THz phase velocity (Hebling et al., 2008b).

Tilted-pulse-front-excitation was suggested to achieve velocity matching for THz generation in LN (Hebling et al., 2002). The operation of this velocity matching method is obvious according to Fig. 11(a). If the intensity front of the excitation pulse is plane, the generated THz radiation will propagate perpendicularly to this plane. This means that for the case of tilted-pulse-front excitation not the group velocity of the pump has to be equal to the THz phase velocity, but the projection of the group velocity into the direction of the THz pulse radiation. So the velocity matching condition can be expressed as:

$$v_{g,p} \cdot \cos\gamma = v_{THz}, \tag{22}$$

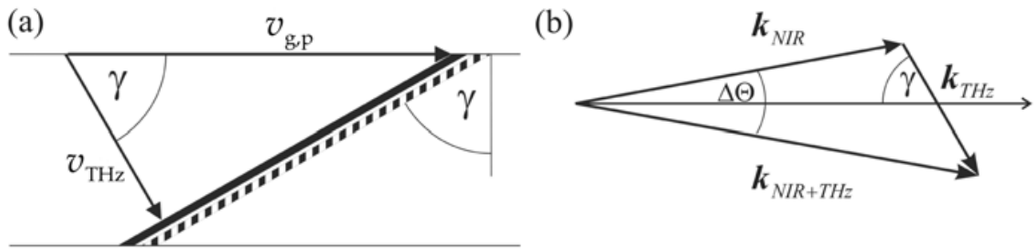

Fig. 11. Velocity matching using tilted-pulse-front excitation. (a) THz wave (bold line) generated in the LN crystal by the tilted intensity front of the pump pulse (dashed bold line) propagates perpendicularly to the THz phase front. (b) Wave-vector diagram for difference-frequency generation (Hebling et al., 2008b).

where $v_{g,p}$ is the group velocity of the pump, and v_{THz} is the phase velocity of the generated THz pulse. According to Eq. (22) an appropriate tilt angle γ can be chosen if the pump velocity is larger than the THz velocity. This is the case for LN.

The first experimental realization of THz-pulse generation by tilted-pulse-front-excitation (Stepanov et al., 2003) resulted in 30-pJ THz pulses for 2-μJ pump pulses. With the same pump energy it was possible to increase the THz energy to 100 pJ by using a better quality (Mg-doped stoichiometric) LN crystal (Hebling et al., 2004). A 200-times increase in the pump energy resulted in 2000 times larger THz energy (Stepanov et al., 2005). Further increasing the pump energy up to the 10-mJ range resulted in THz pulses with energies on the tens-of-μJ range (Yeh et al., 2007, Stepanov et al., 2008). Self-phase modulation of such high-energy THz pulses was observed inside the generating LN crystal (Hebling et al. 2008a). THz pulses with a few μJ energy at 1 kHz repetition rate were successfully used in THz pump-THz probe measurements (Hoffmann et al., 2009, Hebling et al., 2009). In low-bandgap n-type InSb (E_g=0.2 eV) an increase, while in Ge (E_g=0.7 eV) a decrease of the free carrier absorption was observed with sub-ps resolution. The increase in InSb was caused by impact ionization effect created by the electrons energized by the high field of the THz pulses. In Ge having higher bandgap impact ionization was not possible at the achieved field strength. The decrease of absorption was caused by the redistribution of the electrons in the conduction band (Mayer & Keilmann, 1986).

Above we used Fig. 11(a) to explain that for tilted-pulse-front excitation velocity matching is expressed by Eq. (22). On the other hand we know that an angular dispersion according to Eq. (12) is present if the pulse front is tilted and OR can be considered as the result of difference frequency generation (DFG) between individual frequency components of the broadband excitation pulse. In presence of angular dispersion non-collinear DFG occurs. The vector diagram demonstrating phase-matching for non-collinear DFG is depicted in Fig. 11(b). Using Eq. (12), it is easy to show (Hebling et al., 2002) that for small values of $\Delta\varepsilon$ the inclination angle of $\mathbf{k}_{THz}$ from the average propagation direction of the excitation pulse is the same γ as the pulse front tilt angle. Therefore the two pictures used in this section to describe THz pulse excitation by ultrashort pulses with tilted-pulse-front, based on velocity matching and on wave-vector conservation, respectively, predict the same propagation direction for the created THz pulse.

Since for LN there is more than a factor of two between the velocity of the excitation and the velocity of the THz radiation, the tilt angle has to be as large as 63°. According to Eq. (12) this implies a large angular dispersion, and according to Eq. (10) a large GDD. Because of this the duration of the pulse with tilted front is short only in a limited region of space. In order to deal with this problem in THz pulse generation a setup depicted in Fig. 12(a) is used for tilted-pulse-front excitation (Hebling et al. 2004). The necessary angular dispersion is introduced by the grating. The lens images the grating surface to the entrance aperture of the LN crystal. This reproduces the short initial pump pulse duration and high peak power in the image plane inside the crystal, which is essential for efficient THz generation.

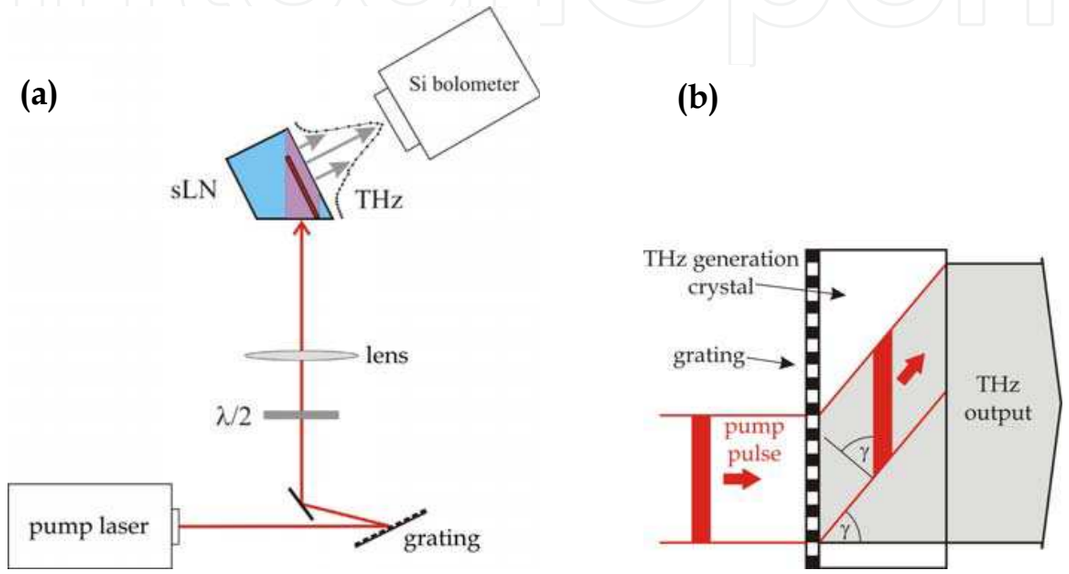

Fig. 12. (a) Experimental setup for THz generation by tilted-pulse-front excitation.
(b) Contact grating scheme.

An important advantage of the TPFP technique is its inherent scalability to higher THz energies. This can be accomplished simply by increasing the pump spot size and energy. However, our detailed analysis (Fülöp et al., 2009) of the pulse-front-tilting setup shows that aberrations caused by the imaging optics can introduce strong asymmetry of the THz beam profile and significant curvature of the THz wavefronts. Such distortions can limit application possibilities of a high-field THz source. In order to overcome the limitations imposed by the imaging optics in the pulse-front-tilting setup we have recently proposed (Pálfalvi et al., 2008) a compact scheme (see Fig. 12(b)), where the imaging optics is omitted and the grating is brought in contact with the crystal.

Besides LN also a few semiconductor materials, such as GaP, GaSe, GaAs, etc., are promising candidates for high-energy THz pulse generation in a contact-grating setup. Due to their lower bandgap as compared to that of LN, semiconductors have to be pumped at longer wavelengths, where only higher-order multiphoton absorption is effective and, as a consequence, higher pump intensities can be used (Fig. 13). In most cases TPFP is necessary for phase matching in semiconductors for longer-wavelength pumping. The required pulse-front-tilt angles are smaller (about 30° or below) than in case of LN, which allow for using larger material thicknesses for THz generation (due to smaller GDD, see above), thereby

compensating for the smaller nonlinear coefficients of semiconductors (Fülöp et al., 2009). In addition, a smaller pulse-front-tilt angle makes the realization of a contact-grating setup technically less challenging. The absorption of LN in the THz range is rapidly increasing with increasing frequency above ca. 1 THz, which makes it less advantageous for generation of higher THz frequencies. The THz absorption of many semiconductors is smaller at higher THz frequencies than that of LN, and they can be used to efficiently generate THz radiation above 1 THz, provided that they are pumped at sufficiently long wavelengths to suppress free-carrier absorption.

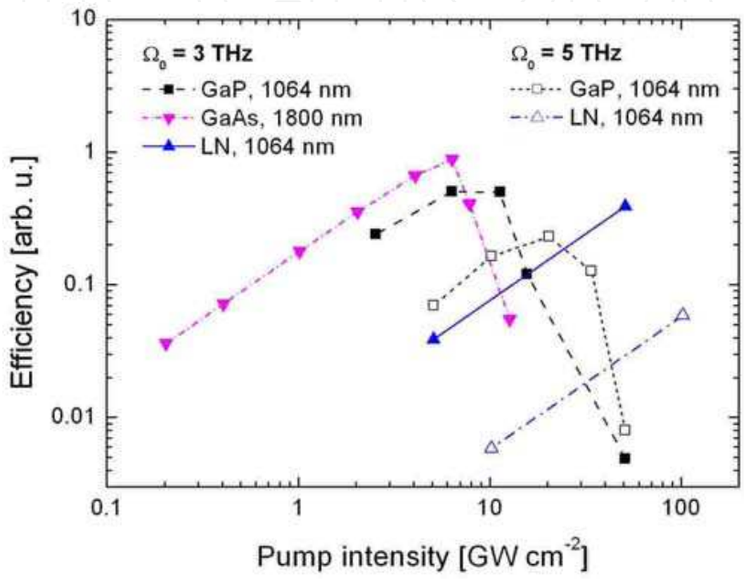

Fig. 13. Calculated maximal THz generation efficiencies in GaP, GaAs and LN for 3 THz and 5 THz phase matching frequencies. The pump wavelength is indicated for each c urve.

6. Conclusion

In summary, a survey on various applications of tilted-pulse-front excitation was given. We have started with considering the relation between pulse front tilt and angular dispersion. It was pointed out that the group velocity can, in general, depend on angular dispersion. Such dependence should be taken into account when considering a beam with angular dispersion propagating as extraordinary wave in a birefringent medium. To our knowledge, this fact was not explicitly mentioned in previous works.

Among the applications of TPFP, which provide an exact synchronization between the pump pulse and the generated excitation along the sample, TWE of visible and x-ray lasers, and ultrafast electron diffraction were briefly reviewed. We have proposed to use a modified pulse front tilting setup for pumping short-wavelength x-ray lasers.

A survey on various nonlinear optical schemes with achromatic phase matching was given including SHG, various types of NOPA and SFG. It was shown that for NOPA with angularly dispersed signal (and the corresponding SFG scheme) achromatic phase matching

is equivalent to simultaneous group velocity and pulse front matching. The importance of this feature to high-power applications was outlined.
Finally, the generation of intense ultrashort THz pulses by OR in LN using TPFP was reviewed, together with applications to ultrafast nonlinear THz spectroscopy. The potential of further upscaling the THz energy and field strength was assessed when using the contact grating scheme with semiconductor materials for OR pumped at IR wavelengths.

7. Note added in proof

After submission of our manuscript, an excellent review paper with a similar topic, but with different emphasis has been published (Torres et al., 2010).

8. Acknowledgement

Financial support from Hungarian Scientific Research Fund (OTKA) grant numbers 76101 and 78262 is acknowledged. Financial support from *Hungarian Scientific Research Fund (OTKA)*, grant numbers 76101 and 78262, and from *Science, Please! Research Team on Innovation (SROP-4.2.2/08/1/2008-0011)* is acknowledged.

9. References

Akturk, S.; Gu, X.; Gabolde, P. & Trebino, R. (2005). The general theory of first-order spatio-temporal distortions of Gaussian pulses and beams. *Opt. Express,* Vol. 13, No. 21, (October 2005) 8642-8660

Barty, C. P. J.; King, D. A.; Yin, G. Y.; Hahn, K. H.; Field, J. E.; Young, J. F. & Harris, S. E. (1988). 12.8-eV laser in neutral cesium. *Phys. Rev. Lett.,* Vol. 61, No. 19, (November 1988) 2201-2204

Baum, P. & Zewail, A. H. (2006). Breaking resolution limits in ultrafast electron diffraction and microscopy. *Proc. Natl. Acad. Sci.,* Vol. 103, No. 44, (October 2006) 16105-16110

Bor, Zs.; Szatmári, S. & Müller, A. (1983). Picosecond pulse shortening by travelling wave amplified spontaneous emission. *Appl. Phys. B,* Vol. 32, No. 3, (November 1983) 101-104

Bor, Zs. & Rácz, B. (1985). Group velocity dispersion in prisms and its application to pulse compression and travelling-wave excitation. *Opt. Commun.,* Vol. 54, No. 3, (June 1985) 165-170

Blanchard, F.; Razzari, L.; Bandulet, H.-C.; Sharma, G.; Morandotti, R., Kieffer, J.-C.; Ozaki, T.; Ried, M.; Tiedje, H. F.; Haugen, H. K. & Hegmann, F. A. (2007). Generation of 1.5 μJ single-cycle terahertz pulses by optical rectification from a large aperture ZnTe crystal. *Opt. Express,* Vol. 15, No. 20, (October 2007) 13212-13220

Cerullo, G. & De Silvestri, S. (2003). Ultrafast optical parametric amplifiers. *Rev. Sci. Instrum.,* Vol. 74, No. 1, (January 2003) 1-18

Daido, H. (2002). Review of soft x-ray laser researches and developments. *Rep. Prog. Phys.,* Vol. 65, (September 2002) 1513-1576

Di Trapani, P.; Andreoni, A.; Solcia, C.; Foggi, P.; Danielius, R.; Dubietis, A. & Piskarskas, A. (1995). Matching of group velocities in three-wave parametric interaction with

femtosecond pulses and application to traveling-wave generators. *J. Opt. Soc. Am. B,* Vol. 12, No. 11, (1 November 1995) 2237-2244

Fülöp, J. A.; Major, Zs.; Henig, A; Kruber, S.; Weingartner, R.; Clausnitzer, T.; Kley, E.-B.; Tünnermann, A.; Pervak, V.; Apolonski, A.; Osterhoff, J.; Hörlein, R.; Krausz, F. & Karsch, S. (2007). Short-pulse optical parametric chirped-pulse amplification for the generation of high-power few-cycle pulses. *New J. Phys.,* Vol. 9, No. 12, (December 2007) 438

Fülöp, J. A.; Pálfalvi, L.; Almási, G. & Hebling, J. (2009). Design of high-energy terahertz sources based on optical rectification. In preparation

Gaal, P.; Reimann, K.; Woerner, M.; Elsaesser, T.; Hey, R. & Ploog, K. H. (2006). Nonlinear terahertz response of n-type GaAs. *Phys. Rev. Lett.*, Vol. 96, No. 18, (May 2006) 187402

Grischkowsky, D.; Keiding, S.; Exter, M. van & Fattinger, Ch. (1990). Far-infrared time-domain spectroscopy with terahertz beams of dielectrics and semiconductors. *J. Opt. Soc. Am. B,* Vol. 7, No. 10, (October 1990) 2006-2015

Harris, S. E. (1969). Tunable optical parametric oscillators. *Proc. IEEE,* Vol. 57, No. 12, (December 1969) 2096-2113

Hebling, J. & Kuhl, J. (1989a). Generation of femtosecond pulses by travelling-wave amplified spontaneous emission. *Opt. Lett.,* Vol. 14, No. 5, (March 1989) 278-280

Hebling, J. & Kuhl, J. (1989b). Generation of tunable femtosecond pulses by travelling wave amplification. *Opt. Commun.,* Vol. 73, No. 5 (November 1989) 375-379

Hebling, J.; Kuhl, J. & Klebniczki, J. (1991). Femtosecond optical gating with a traveling-wave amplifier. *J. Opt. Soc. Am. B,* Vol. 8, No. 5, (May 1991) 1089-1092

Hebling, J. (1996). Derivation of the pulse front tilt caused by angular dispersion. *Opt. Quantum Electron.,* Vol. 28, No. 12, (December 1996) 1759-1763

Hebling, J.; Almási, G.; Kozma, I. Z. & Kuhl, J. (2002).Velocity matching by pulse front tilting for large area THz-pulse generation. *Opt. Express,* Vol. 10, No. 21, (October 2002) 1161-1166

Hebling, J.; Stepanov, A.G.; Almási, G.; Bartal, B. & Kuhl, J. (2004). Tunable THz pulse generation by optical rectification of ultrashort laser pulses with tilted pulse fronts. *Appl. Phys. B,* Vol. 78, No. 5, (March 2004) 593–599

Hebling, J.; Yeh, K.-L.; Hoffmann, M. C. & Nelson, K. A. (2008a). High-power THz generation, THz nonlinear optics, and THz nonlinear spectroscopy. *IEEE J. Sel. Top. Quantum Electron.*, Vol. 14, No. 2, (March-April 2008) 345-353

Hebling, J.; Yeh, K.-L.; Hoffmann, M. C.; Bartal, B. & Nelson, K. A. (2008b). Generation of high-power terahertz pulses by tilted-pulse-front excitation and their application possibilities. *J. Opt. Soc. Am. B,* Vol. 25, No. 7, (July 2008) 6-19

Hebling, J.; Hoffmann, M. C.; Hwang, H. Y.; Yeh, K.-L. & Nelson, K. A. (2009). Comparison of Nonequilibrium Carrier Distribution in Ge, Si and GaAs observed by THz-Pump/THz-Probe Measurements. *Phys. Rev. B,* (submitted)

Hoffmann, M. C., Yeh, K.-L.; Hebling, J. & Nelson, K. A. (2007). Efficient terahertz generation by optical rectification at 1035 nm. *Opt. Express,* Vol. 15, No. 18, (September 2007) 11706-11713

Hoffmann, M. C.; Hebling, J.; Hwang, H. Y.; Yeh, K.-L. & Nelson, K. A. (2009). Impact ionization in InSb probed by terahertz pump-terahrtz probe spectroscopy. *Phys. Rev. B,* Vol. 79, No. 16 (April 2009) 161201 (R)

Hofmann, Th.; Mossavi, K.; Tittel, F. K. & Szabó, G. (1992). Spectrally compensated sum-frequency mixing scheme for generation of broadband radiation at 193 nm. *Opt. Lett.,* Vol. 17, No. 23, (1 December 1992) 1691-1693

Hu, B. B.; Zhang, X.-C. & Auston, D. H. (1990). Free-space radiation from electro-optical crystals. *Appl. Phys. Lett.,* Vol. 56, No. 6, (February 1990) 506-508

Kapteyn, H. C. (1992). Photoionization-pumped x-ray lasers using ultrashort-pulse excitation. *Appl. Opt.,* Vol. 31, No. 24, (August 1992) 4931-4939

Kawachi, T.; Kado, M.; Tanaka, M.; Sasaki, A.; Hasegawa, N.; Kilpio, A. V.; Namba, S.; Nagashima, K.; Lu, P.; Takahashi, K.; Tang, H.; Tai, R.; Kishimoto, M.; Koike, M.; Daido, H. & Kato, Y. (2002). Gain saturation of nickel-like silver and tin x-ray lasers by use of a tabletop pumping laser system. *Phys. Rev. A,* Vol. 66, No. 3, (September 2002) 033815

Klebniczki, J.; Hebling, J. & Kuhl, J. (1990). Generation of tunable femtosecond pulses in a traveling-wave amplifier. *Opt. Lett.,* Vol. 15, No. 23, (December 1990) 1368-1370

Kobayashi, T. & Shirakawa, A. (2000). Tunable visible and near-infrared pulse generation in a 5 fs regime. *Appl. Phys. B,* Vol. 70, Supplement 1, (June 2000) S239-S246

Kozma, I. Z.; Almási, G. & Hebling, J. (2003). Geometrical optical modeling of femtosecond setups having angular dispersion. *Appl. Phys. B,* Vol. 76, No. 3, (March 2003) 257-261

Lee, Y.-S. (2009). *Principles of Terahertz Science and Technology,* Springer Science+ Business Media, LLC, ISBN: 978-0-387-09539-4, e-ISBN: 978-0-387-09540-0, New York

Löffler, T.; Hahn, T.; Thomson, M.; Jacob, F. & Roskos, H. G. (2005). Large-area electro-optic ZnTe terahertz emitters. *Opt. Express,* Vol. 15, No. 9, (April 2005) 5353-5362

Main, I. G. (1978). *Vibrations and Waves in Physics,* Cambridge University Press, ISBN 0-521-216621-1, Cambridge

Major, Zs.; Trushin, S. A.; Ahmad, I; Siebold, M.; Wandt, C.; Klingebiel, S.; Wang, T.-J.; Fülöp, J. A.; Henig, A.; Kruber, S.; Weingartner, R.; Popp, A.; Osterhoff, J.; Hörlein, R.; Hein, J.; Pervak, V.; Apolonski, A.; Krausz, F. & Karsch S. (2009). Basic concepts and current status of the Petawatt Field Synthesizer –A new approach to ultrahigh field generation. *The Review of Laser Engineering,* Vol. 37, No. 6, (June 2009) 431-436

Martínez, O. E.; Gordon, J., P. & Fork, R., L. (1984). Negative group-velocity dispersion using refraction. *J. Opt. Soc. Am A,* Vol. 1, No. 10, (October 1984) 1003-1006

Martínez, O. E. (1986). Pulse distortions in tilted pulse schemes for ultrashort pulses. *Opt. Commun.,* Vol. 59, No. 3, (September 1986) 229-232

Martínez, O. E. (1989). Achromatic phase matching for second harmonic generation of femtosecond pulses. *IEEE J. Quantum Electron.,* Vol. 25, No. 12, (December 1989) 2464-2468

Mayer, A. & Keilmann, F. (1986). Far-infrared nonlinear optics. II. $\chi^{(3)}$ contributions from the dynamics of free carriers in semiconductors. *Phys. Rev. B,* Vol. 33, No. 10, (15 May 1986) 6962-6968

Pálfalvi, L.; Fülöp, J. A.; Almási, G. & Hebling, J. (2008). Novel setups for extremely high power single-cycle terahertz pulse generation by optical rectification. *Appl. Phys. Lett.,* Vol. 92, No. 17, (28 April 2008) 171107

Polland, H. J.; Elsaesser, T.; Seilmeier, A.; Kaiser, W.; Kussler, M.; Marx, N. J.; Sens, B. & Drexhage, K. H. (1983). Picosecond dye laser emission in the infrared between 1.4 and 1.8 μm. *Appl. Phys. B,* Vol. 32, No. 2, (October 1983) 53-57

Richman, B. A.; Bisson, S. E.; Trebino, R.; Sidick, E. & Jacobson, A. (1998). Efficient broadband second-harmonic generation by dispersive achromatic nonlinear conversion using only prisms. *Opt. Lett.,* Vol. 23, No. 7, (April 1998) 497-499

Saikan, S. (1976). Automatically tunable second-harmonic generation of dye lasers. *Opt. Commun.,* Vol. 18, No. 4, (September 1976) 439-443

Schiller, N. H. & Alfano, R. R. (1980). Picosecond characteristics of a spectrograph measured by a streak camera/video readout system. *Opt. Commun.,* Vol. 35, No. 3, (December 1980) 451-454

Sher, M. H.; Macklin, J. J.; Young, J. F. & Harris, S. E. (1987). Saturation of the Xe III 109-nm laser using traveling-wave laser-produced-plasma excitation. *Opt. Lett.,* Vol. 12, No. 11, (November 1987) 891-893

Simon, P.; Földes, I. B. & Szatmári, S. (2005). Laser-induced x-rays and x-ray lasers. *A kvantumoptika és –elektronika legújabb eredményei,* ELFT Atom-, Molekulafizikai és Kvatnumelektronikai Szakcsoport, Tavaszi Iskola 2005. május 31- június 3. Balatonfüred (in Hungarian)

Stepanov, A. G.; Hebling, J. & Kuhl, J. (2003). Efficient generation of subpicosecond terahertz radiation by phase-matched optical rectification using ultrashort laser pulses with tilted pulse fronts. *Appl. Phys. Lett.,* Vol. 83, No. 15, (October 2003) 3000-3002

Stepanov, A. G.; Kuhl, J.; Kozma, I. Z.; Riedle, E.; Almási, G. & Hebling, J. (2005). Scaling up the energy of THz pulses created by optical rectification. *Opt. Express,* Vol. 13, No. 15, (July 2005) 5762-5768

Stepanov, A. G.; Bonacina L.; Chekalin S. V. & Wolf, J.-P. (2008). Generation of 30 μJ single-cycle terahertz pulses at 100 Hz repetition rate by optical rectification. *Opt. Lett.* Vol. 33, No. 21, (November 2008) 2497-2499

Szabó, G.; Rácz, B.; Müller, A.; Nikolaus, B. & Bor, Zs. (1984). Travelling-wave-pumped ultrashort-pulse distributed-feedback dye laser. *Appl. Phys. B,* Vol. 34, No. 3, (March 1984) 145-147

Szabó, G. & Bor, Zs. (1990). Broadband frequency doubler for femtosecond pulses. *Appl. Phys. B,* Vol. 50, No. 1, (January 1990) 51-54

Szabó, G. & Bor, Zs. (1994). Frequency conversion of ultrashort pulses. *Appl. Phys. B,* Vol. 58, No. 3, (March 1994) 237-241

Szatmári, S.; Kuhnle, G. & Simon, P. (1990). Pulse compression and traveling wave excitation scheme using a single dispersive element. *Appl. Opt.,* Vol. 29, No. 36, (December 1990) 5372-5379

Tonouchi, M. (2007). Cutting-edge terahertz technology. *Nature Photonics,* Vol. 1, No. 2, (February 2007) 97-105

Topp, M. R. & Orner, G. C. (1975). Group dispersion effects in picosecond spectroscopy. *Opt. Commun.,* Vol. 13, No. 3, (March 1975) 276-281

Torres, J. P.; Hendryc, M. & Valencia, A. (2010). Angular Dispersion: an enabling tool in nonlinear and quantum optics. Adv. Opt. Photonics, submitted

Yeh, K.-L.; Hoffmann, M. C.; Hebling, J. & Nelson, K. A. (2007). Generation of 10 μJ ultrashort terahertz pulses by optical rectification. *Appl. Phys. Lett.,* Vol. 90, No. 17, (April 2007) 171121

Zhang, T. R.; Choo, H. R. & Downer, M. C. (1990). Phase and group velocity matching for second harmonic generation of femtosecond pulses. *Appl. Opt.,* Vol. 29, No. 27, (September 1990) 3927-3933

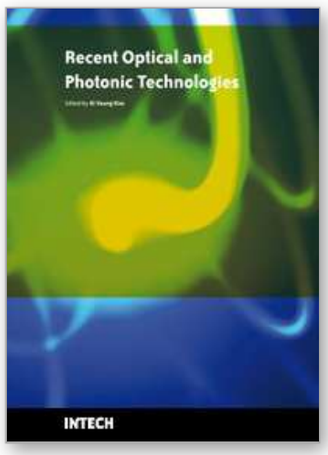

Recent Optical and Photonic Technologies

Edited by Ki Young Kim

ISBN 978-953-7619-71-8
Hard cover, 450 pages
Publisher InTech
Published online 01, January, 2010
Published in print edition January, 2010

Research and development in modern optical and photonic technologies have witnessed quite fast growing advancements in various fundamental and application areas due to availability of novel fabrication and measurement techniques, advanced numerical simulation tools and methods, as well as due to the increasing practical demands. The recent advancements have also been accompanied by the appearance of various interdisciplinary topics. The book attempts to put together state-of-the-art research and development in optical and photonic technologies. It consists of 21 chapters that focus on interesting four topics of photonic crystals (first 5 chapters), THz techniques and applications (next 7 chapters), nanoscale optical techniques and applications (next 5 chapters), and optical trapping and manipulation (last 4 chapters), in which a fundamental theory, numerical simulation techniques, measurement techniques and methods, and various application examples are considered. This book deals with recent and advanced research results and comprehensive reviews on optical and photonic technologies covering the aforementioned topics. I believe that the advanced techniques and research described here may also be applicable to other contemporary research areas in optical and photonic technologies. Thus, I hope the readers will be inspired to start or to improve further their own research and technologies and to expand potential applications. I would like to express my sincere gratitude to all the authors for their outstanding contributions to this book.

INTECH
open science | open minds

InTech Europe
University Campus STeP Ri
Slavka Krautzeka 83/A
51000 Rijeka, Croatia
Phone: +385 (51) 770 447
Fax: +385 (51) 686 166

InTech China
Unit 405, Office Block, Hotel Equatorial Shanghai
No.65, Yan An Road (West), Shanghai, 200040, China
中国上海市延安西路65号上海国际贵都大饭店办公楼405单元
Phone: +86-21-62489820
Fax: +86-21-62489821

IntechOpen

IntechOpen